Calculations of the structure of basin volumes for mechanically stable packings

S. S. Ashwin,[1,2] Jerzy Blawzdziewicz,[3] Corey S. O'Hern,[1,2] and Mark D. Shattuck[4]
[1]*Department of Mechanical Engineering and Materials Science, Yale University, New Haven, Connecticut 06520-8286, USA*
[2]*Department of Physics, Yale University, New Haven, Connecticut 06520-8120, USA*
[3]*Department of Mechanical Engineering, Texas Tech University, Lubbock, Texas 74909-1021, USA*
[4]*Benjamin Levich Institute and Physics Department, The City College of the City University of New York, New York, New York 10031, USA*
(Received 18 December 2011; revised manuscript received 4 April 2012; published 19 June 2012)

Experimental and computational model systems composed of frictionless particles in a fixed geometry have a finite number of distinct mechanically stable (MS) packings. The frequency of occurrence for each MS packing is highly variable and depends strongly on preparation protocol. Despite intense work, it is extremely difficult to predict *a priori* the MS packing probabilities. We describe a novel computational method for calculating the volume and other geometrical properties of the "basin of attraction" for each MS packing. The basin of attraction for an MS packing contains all initial conditions in configuration space that map to that MS packing using a given preparation protocol. We find that the basin is a highly complex structure. For a compressive-quench-from-zero-density protocol, we show the existence of a small core volume of the basin around each MS packing for which *all points* map to that MS packing. However, in contrast to previous studies for supercooled liquids, glasses, and over-compressed jammed systems, we find that the MS packing probabilities are very weakly correlated with this core volume. Instead, MS packing probabilities obtained from compression protocols that use initially dilute configurations and do not allow particle overlaps (i.e., those relevant to granular media) are determined by complex geometric features of the basin of attraction that are distant from the MS packing. In particular, we find that the shape of the average basin profile function $S(l)$, which gives the probability for a point on a hyperspherical shell a distance l from a given MS packing to map back to that packing, can be described by a Γ distribution with a peak that increases as the system size increases and as the quench rate decreases. We find a simple model which predicts $S(l)$ for the extreme cases of very slow and fast quench rates.

DOI: 10.1103/PhysRevE.85.061307 PACS number(s): 83.80.Fg, 63.50.Lm, 61.43.−j, 64.70.ps

I. INTRODUCTION

In contrast to equilibrium, thermal systems, the structural and mechanical properties of dense granular materials and other athermal particulate systems depend strongly on the protocol used to create them. For example, a number of studies have shown that the packing fraction of granular assemblies can vary from values associated with random loose [1] to random close packing [2] as a function of the vibration amplitude and tapping history [3,4]. In addition, the force chain networks that form, and thus the shear modulus of granular packings depend on whether they have been generated via shear, isotropic compression [5], or sedimentation via single-particle or collective deposition [6].

The protocol dependence in dense granular systems arises from the nonlinear, dissipative, and frictional contact interactions between grains [7]. Despite active research in this area, the distinct contributions from each of these interactions to protocol dependence has not been determined. In this manuscript, we investigate the protocol dependence of static granular packings by focusing on a simple system of frictionless spherical particles that interact via purely repulsive linear spring and velocity-dependent damping forces. For a fixed set of boundary conditions, there is a finite number of distinct mechanically stable (MS) packings of frictionless particles, which grows exponentially with the number of particles N [8]. MS packings exist as discrete points in configuration space that are characterized by the packing fraction ϕ_J and N particle coordinates $\vec{R}_J = \{\vec{r}_1, \vec{r}_2 \ldots \vec{r}_N\}$ and coincide with local minima of the density landscape [9,10] (or local minima of the potential energy landscape with zero potential $V = 0$). We have shown recently in both simulations and experiments that the probabilities with which these distinct MS packings occur are highly nonuniform and depend on parameters of the packing-generation protocol including the compression rate, damping coefficient, and initial packing fraction [11,12]. However, one cannot yet determine *a priori* which MS packings are the most versus the least probable, much less calculate the packing probabilities as a function of the packing-generation protocol. The ability to calculate MS packing probabilities and, more specifically, the probability for particular rigid structural motifs or patterns [13,14] to occur is essential for developing a statistical mechanicslike description of granular packings.

Here, we describe a novel method for calculating the MS packing probabilities by measuring the volume of the MS packing "basin of attraction," which we define as the collection of initial points in configuration space (i.e., the dark-shaded region in Fig. 1) at *zero packing fraction* that map to a given MS packing by following a compressive-quench-from-zero-density protocol (which corresponds to dynamics on the density landscape and is described in detail in Sec. II). Note that our definition of the basin of attraction is protocol dependent, and thus the basin volume will vary with the rate at which energy is dissipated, the compression rate, and other parameters. In contrast, basins of attraction for supercooled and glassy liquids [15] and overcompressed jammed systems [16] have been defined as the set of initial dense liquid configurations that map to the "nearest" local minimum using steepest descent dynamics at fixed density. Our definition of basin volumes is directly relevant for granular systems (as well

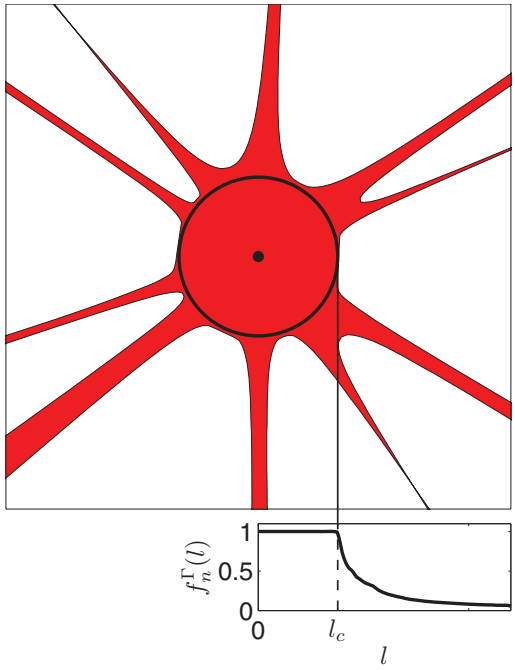

FIG. 1. (Color online) (Top) A schematic of the basin of attraction (dark-shaded region) in dN-dimensional configuration space for a typical mechanically stable packing (black dot). (Bottom) The corresponding unweighted basin profile function $f_n^\Gamma(l)$ is plotted as a function of distance l from MS packing n for packing-generation protocol Γ. $f_n^\Gamma(l)$ begins to decay from 1 beyond an approximately spherically symmetric core size l_c, while for $l > l_c$ the basin is highly branched, threadlike, and $f_n^\Gamma(l) \to 0$.

as athermal polymer packings [17–20]), in which MS packings are generated from initially dilute configurations followed by compression and relaxation, where particle overlaps are negligible during the relaxation process and in the final MS packing.

Calculating MS packing basin volumes is a computationally complex problem because the average basin volume scales as e^{-N}, and the number of basins grows exponentially e^N, where N is the number of particles. Thus, random sampling of configuration space will not yield accurate measurements of MS packing basin volumes in the large-N limit [16,21]. To aid in the calculation of the basin volumes, we introduce the unweighted basin profile function $f_n^\Gamma(l)$, which is the fraction of points on a hypersurface in configuration space a distance l from the nth MS packing that maps via a given dynamics (labeled Γ) to MS packing n.

We will show that there is a hyperspherical core region surrounding each MS packing in which $f_n^\Gamma(l) = 1$ for $l \leqslant l_c$, while $f_n^\Gamma(l) < 1$ for $l > l_c$. Further from the MS packing, the basin becomes highly branched, threadlike, and $f^\Gamma(l) \to 0$ (see Fig. 1.) This picture raises several key questions: (1) Are the MS packing packing probabilities determined by the size l_c of the core region in configuration space or dominated by contributions far from the MS packing, (2) what are the geometrical properties of the basins of attraction, and (3) do their morphologies depend sensitively on the packing-generation protocol? We will show below that the MS packing probabilities are not strongly correlated with the volume of the core regions in configuration space and are instead determined by features of the density landscape that are far from each MS packing. Despite this, we are able to predict the protocol- and system-size dependence of the average basin profile function, which determines the MS packing probabilities.

II. METHODS

To perform our calculations of basin volumes, we focused on a well-characterized model system composed of N frictionless disks in two dimensions that interact via purely repulsive linear spring and velocity-dependent damping forces. N is varied from 3 to 100, and the particles are enclosed in a square cell with fixed walls of length $L = 1$. Interactions with the walls match those between the particles. We consider both monodisperse and bidisperse systems, where the bidisperse mixtures contain half large and half small disks ($N_s = N_l = N/2$) with diameter ratio $\sigma_l/\sigma_s = 1.4$.

In a number of previous studies, we described the MS "packing finder" that generates a mechanically stable packing via isotropic compression at ϕ_J with infinitesimal overlap from an arbitrary initial condition at $\phi = 0$ [11]. Briefly, the algorithm includes the following steps. For each trial, we initialize the system with random particle positions inside the unit square at $\phi = 0$ and zero velocities. We then compress the system in steps of $\Delta\phi = 10^{-4}$ and relax the small particle overlaps after each step by solving Newton's equations of motion with damping,

$$m\vec{a}_i = \sum_j \vec{F}(r_{ij}) - b\vec{v}_i, \tag{1}$$

where m, σ, and $\vec{a}_i$ are the particle mass, diameter, and acceleration,

$$\vec{F}(r_{ij}) = \frac{\epsilon}{\sigma}\left(1 - \frac{r_{ij}}{\sigma}\right)\Theta\left(1 - \frac{r_{ij}}{\sigma}\right)\hat{r}_{ij}, \tag{2}$$

ϵ is the characteristic energy scale of the repulsive spring force $\vec{F}(r_{ij})$ [22], $\Theta(x)$ is the Heaviside step function, $\widetilde{b} = b\sigma/\sqrt{m\epsilon}$ is the damping coefficient, $\hat{r}_{ij}$ is the unit vector connecting the centers of particles i and j, and r_{ij} is their separation, until the kinetic energy per particle falls below a specified tolerance $K/\epsilon N < K_{\rm tol} = 10^{-25}$. We studied a wide range of values for the damping coefficient from $\widetilde{b} = 10^{-2}$ to 10, which mimics steepest descent dynamics. The packing-generation algorithm terminates when the minimized total potential energy per particle $V/\epsilon N > V_{\rm tol} = 10^{-16}$. As in previous studies on similar systems with periodic boundary conditions, we distinguish MS packings based on the spectrum of nontrivial eigenvalues of the dynamical matrix [12], and we find that the number of distinct MS packings $\mathcal{N}_s$ grows exponentially with N as shown in Table I. The $\mathcal{N}_s = 6$ and 80 distinct MS packings for $N = 4$ and 6 are shown in Figs. 2 and 3. The light-shaded (blue) particles form the force-bearing backbones of the mechanically stable packings. The dark-shaded (red) particles are "rattlers" with fewer than three particle-particle or particle-wall contacts. The packing finder does produce a small number of unstable packings as shown in the upper left corner in Fig. 2, but these are not included in the analyses.

TABLE I. The number of distinct mechanically stable packings $\mathcal{N}_s$ and total number of microstates $\mathcal{N}_m$ versus the number of particles N. For $N = 3$ we consider monodisperse systems. For the other system sizes, results are given for bidisperse mixtures. For $N = 12$ we estimate $\mathcal{N}_s$ and $\mathcal{N}_m$. We do not include unstable packings such as the one in the upper left corner of Fig. 2 in which the "rigid backbone" of light-shaded (green) particles can translate.

N	$\mathcal{N}_s$	$\mathcal{N}_m$
2	1	4
3	1	24
4	6	136
6	80	19440
12	∼12 000	$\sim 4 \times 10^{10}$

The fundamental quantity in our approach is the unweighted basin profile function $f_n^\Gamma(l)$ defined as

$$f_n^\Gamma(l) = \int d\vec{R} G_\Gamma(\vec{R}, \vec{R}_J^n) \delta(|\vec{R} - \vec{R}_J^n| - l), \qquad (3)$$

where $f_n^\Gamma(l)$ is sampled on hyperspherical shells a distance l from MS packing n, Γ is the specified compression dynamics, $\delta(x)$ is the Dirac delta function, $G_\Gamma(\vec{R}, \vec{R}_J^n) = 1$ for points $\vec{R}$ in configuration space that map to MS packing $\vec{R}_J^n$, and 0 otherwise. As an illustrative example, we calculate slices of $G_\Gamma(\vec{R}, \vec{R}_J^n)$ for $N = 3$, which has a single MS packing with

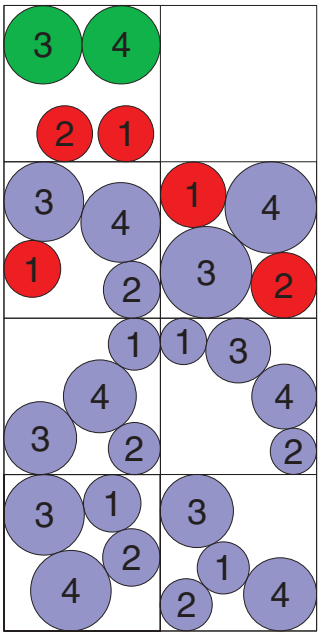

FIG. 2. (Color online) The bottom six configurations are the $\mathcal{N}_s = 6$ distinct mechanically stable packings for bidisperse systems with $N = 4$. (We will refer to configurations 1 through 6 counting in ascending order from left to right and bottom to top.) The light-shaded (blue) particles form the force-bearing backbones of the mechanically stable packings. The dark-shaded (red) particles are "rattlers" with fewer than three particle-particle or particle-wall contacts. The packing finder generates a small number of unstable configurations similar to that shown in the upper left corner with probability less than 0.2%, but these are not included in the analyses.

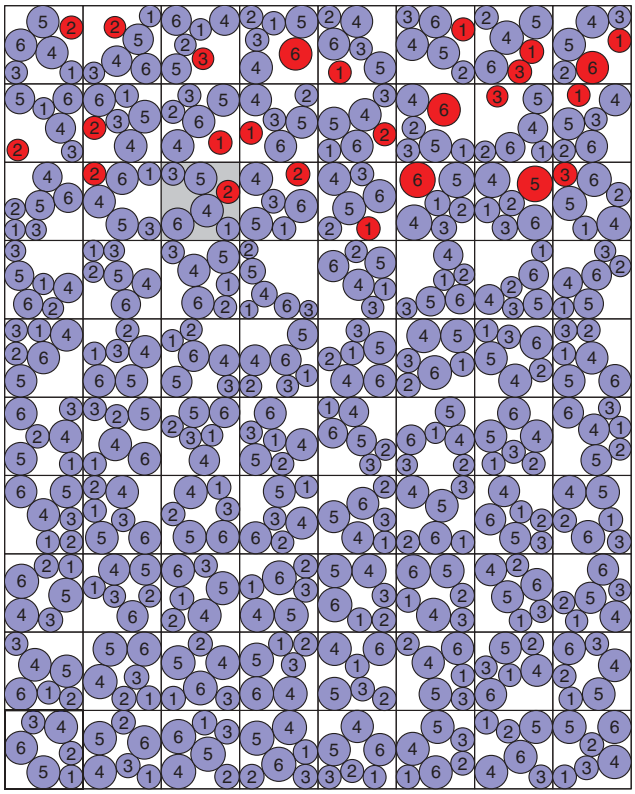

FIG. 3. (Color online) The $\mathcal{N}_s = 80$ distinct mechanically stable packings for bidisperse systems with $N = 6$. The light-shaded (blue) particles form the force-bearing backbones of the mechanically stable packings. The dark-shaded (red) particles are "rattlers" with fewer than three contacts. The unweighted and weighted basin profile functions are shown in Fig. 13 for the configuration in the third row that is shaded gray.

$\mathcal{N}_m = 24$ microstates, (i.e., six particle-label permutations and four polarizations obtained by applying all possible reflections and rotations in two dimensions consistent with the square cell boundary conditions [12]). In Fig. 4, we plot the microstate basins of the attraction $\sum_{n=1}^{\mathcal{N}_m} nG(\{\vec{r}_1, \vec{r}_2^0, \vec{r}_3^0\}, \vec{R}_J^n)$ for fixed $\vec{r}_2^0 = (0.2, 0.6)$ and $\vec{r}_3^0 = (0.45, 0.85)$.

We calculate the unweighted basin profile function $f_n^\Gamma(l)$ using two procedures; the first method is efficient and accurate for small l and the second for large l. For method 1, we generate at least $M = 10^6$ points randomly on the surface of a $2N$-dimensional hypersphere centered on the MS packing with radius l. We then input each of these configurations as initial configurations into the MS packing finder with packing fraction $\phi_i = 0$. If a given initial condition belongs to the basin of attraction of MS packing n, the packing finder will generate packing n. Otherwise, the initial condition belongs to a different basin. For the system sizes where we can achieve complete enumeration, we found that the criterion, $\max_i (d_i^j - d_i^k)/d_i^k < 10^{-6}$, was sufficiently sensitive to distinguish MS packings, where d_i^j is the ith sorted eigenvalue of the dynamical matrix for MS packing j. From method 1, the unweighted basin profile function for MS

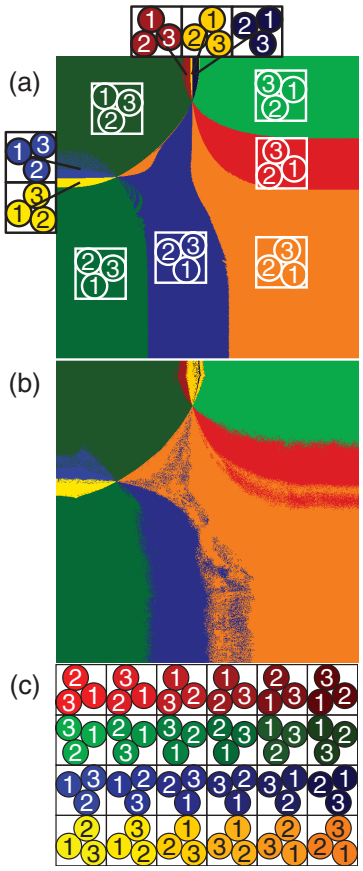

FIG. 4. (Color) The microstate basins of attraction for a system of three monodisperse frictionless disks, where particles 2 and 3 are initially located at positions (0.2,0.6) and (0.45,0.85) in the x-y plane (with the origin in the lower left corner). Results are shown for two damping coefficients, (a) $\widetilde{b} = 1$ and (b) $\widetilde{b} = 0.1$. The position of each pixel represents the initial position of particle 1 and its color corresponds to one of the 11 out of 24 microstates in (c) to which the system evolved under the compression protocol. For $N = 3$ monodisperse systems, there is one distinct MS packing ($\mathcal{N}_s = 1$) with four polarizations (hue; rows) and six permutations (saturation; columns) for a total of $\mathcal{N}_m = 24$ microstates.

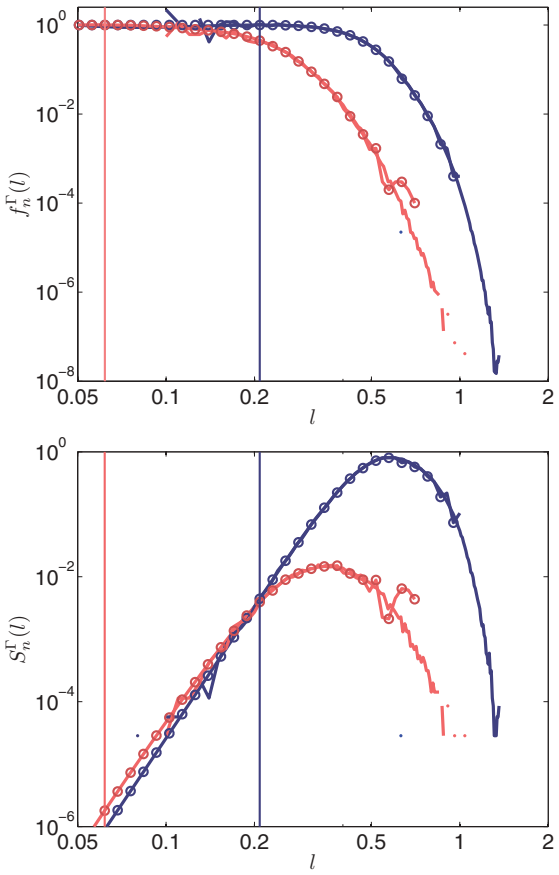

FIG. 5. (Color online) (Top) The unweighted $f_n^\Gamma(l)$ and (bottom) weighted $S_n^\Gamma(l)$ basin profile functions measured for $N = 4$ and $\widetilde{b} = 1$ using methods 1 (circles) and 2 (solid lines) for MS packings 1 (highest probability; dark blue line) and 4 (lowest probability; light red line) shown in Fig. 2. The vertical lines indicate l_c for each MS packing.

packing n is

$$f_n^\Gamma(l) = \frac{M_n}{M}, \tag{4}$$

where M_n is the number of initial conditions at l that map to to packing n.

We define the basin volume for MS packing n generated using compression dynamics Γ as

$$V_n = \int_0^{\sqrt{2N}} S_n^\Gamma(l) dl, \tag{5}$$

where

$$S_n^\Gamma(l) = A_{2N} f_n^\Gamma(l) l^{2N-1} \mathcal{P}_n N_s! N_l! \tag{6}$$

is the (angle-averaged) weighted basin profile function, $A_k = 2\pi^{k/2}/\Gamma(k/2)$ is the surface area of a k-dimensional unit sphere, and $\mathcal{P}_n$ is the number of distinct polarizations for MS packing n [12]. The probability of MS packing n for a given compression protocol Γ is proportional to its basin volume, $P_n^\Gamma = V_n^\Gamma / V_{\rm tot}$, where $V_{\rm tot} = \sum_{n=1}^{\mathcal{N}_s} V_n^\Gamma = L^{2N} = 1$.

Method 1 becomes inefficient at calculating $f_n^\Gamma(l)$ for large $l > l_c$ because the ratio of the area of the intersection of the basin with the hypersphere to the area of the hypersphere becomes extremely small. Thus, in this regime we implement method 2, which was previously employed to calculate the probabilities P_n^Γ directly [8]. For this method, we generate at least 10^6 random points in configuration space and input these into the packing finder with $\phi_i = 0$. The fraction of random initial configurations that map to MS packing n determines P_n^Γ. We can then calculate $f_n^\Gamma(l)$ from P_n^Γ using Eqs. (5) and (6). Note that an advantage of method 2 is that each initial condition provides information about P_n^Γ for some n and for $N_s! N_l!$ distances l by permuting the labels of the final MS packing. See the Appendix for the effects of rattler particles on the unweighted basin profile function $f_n^\Gamma(l)$.

III. RESULTS

Typical basin profile functions $f_n^\Gamma(l)$ are shown for the most and least probable MS packings (1 and 4 in Fig. 2) for $N = 4$ in the top panel of Fig. 5. For small distances from the MS packing $l < l_c$, $f_n^\Gamma(l) = 1$. Beyond the core size l_c, which can

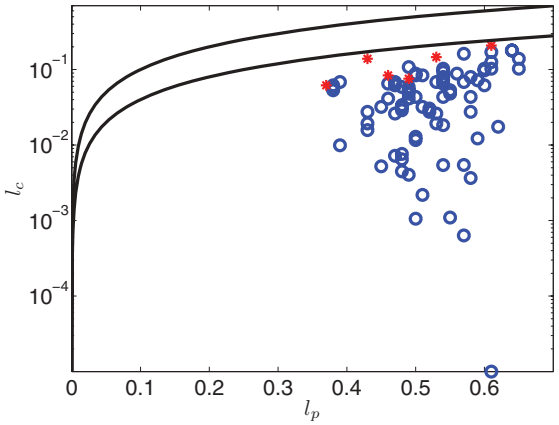

FIG. 6. (Color online) The distance l_c beyond which the unweighted basin profile function $f_n^\Gamma(l) < 1$ plotted versus the location of the peak l_p in the weighted basin profile function $S_n^\Gamma(l)$ for each MS packing for $N = 4$ (asterisks) and 6 (circles) obtained using method 1 with damping parameter $\widetilde{b} = 1$. The solid lines indicate $l_c = l_p$ (top) and $l_c = 0.4 l_p$ (bottom).

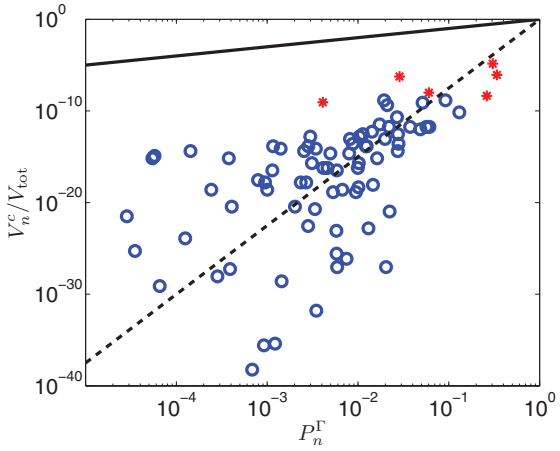

FIG. 7. (Color online) The volume V_n^c of the hyperspherical cores surrounding each MS packing n (relative to $V_{\rm tot}$) plotted as a function of the MS packing probability P_n^Γ for each MS packing for $N = 4$ (asterisks) and 6 (circles) obtained using method 1 with damping parameter $\widetilde{b} = 1$. The solid (dashed) line has slope 1 (7.5).

vary strongly from one MS packing to another, $f_n^\Gamma(l)$ decays rapidly to zero. In the bottom panel of Fig. 5, we show the weighted basin profile $S_n^\Gamma(l)$ for the same $N = 4$ MS packings. Since $S_n^\Gamma(l)$ is obtained by multiplying $f_n^\Gamma(l)$ by l^{2N-1}, the probabilities for obtaining MS packings (when starting from zero packing fraction) are determined by distances $l > l_c$. For $N = 4$, the average and maximum core sizes are $\langle l_c \rangle \approx 0.1$ and $l_c^{\rm max} = 0.21$, and the small particle diameter is $\sigma = 0.3$, but the average length scale that yields 50% of the packing probabilities [near the peak in $S_n^\Gamma(l)$] is $\langle l_p \rangle \approx 0.5$. We find that $l_c/l_p < 1$ for all MS packings for $N = 4$ and 6 as shown in Fig. 6. We have validated these results by ensuring that methods 1 and 2 yield the same values for $f_n^\Gamma(l)$ and $S_n^\Gamma(l)$ over the range in l in which the calculations overlap.

In the top panel of Fig. 5, we show that the core size for the most probable $N = 4$ MS packing is larger than that for the least probable MS packing, which may suggest that there is a correlation between the core size and the MS packing probabilities. To investigate to what extent the hyperspherical core surrounding each MS packing determines the packing probabilities, we approximate the basin volume by the volume of a hypersphere of radius l_c, $V_n^c = \pi^N l_c^{2N}/\Gamma(N+1)$, for each MS packing. In Fig. 7, we plot $V_n^c/V_{\rm tot}$ versus P_n^Γ for $N = 4$ and 6. We find two key results: (1) The volumes $V_n^c/V_{\rm tot}$ are smaller by many orders of magnitude than the probabilities P_n^Γ and (2) a power-law fit to the data for $N = 6$ yields $V_n^c/V_{\rm tot} \sim (P_n^\Gamma)^\lambda$ with $\lambda \approx 7.5$, but there is only a very weak correlation between $V_n^c/V_{\rm tot}$ and the packing probabilities [11]. For example, the scatter in the data can vary by more than 20 orders of magnitude! Thus, features of the basin geometrical structure beyond the core region control the MS packing probabilities for packings that are generated from dilute initial configurations.

To begin to investigate the nature of the basin morphology beyond the core region, we characterize in detail the shapes of the weighted basin profile functions for each of the $\mathcal{N}_s$ MS packings for $N = 6$ in Fig. 8(a). As found for the distribution of Voronoi volumes in dense granular packings [23–25], the

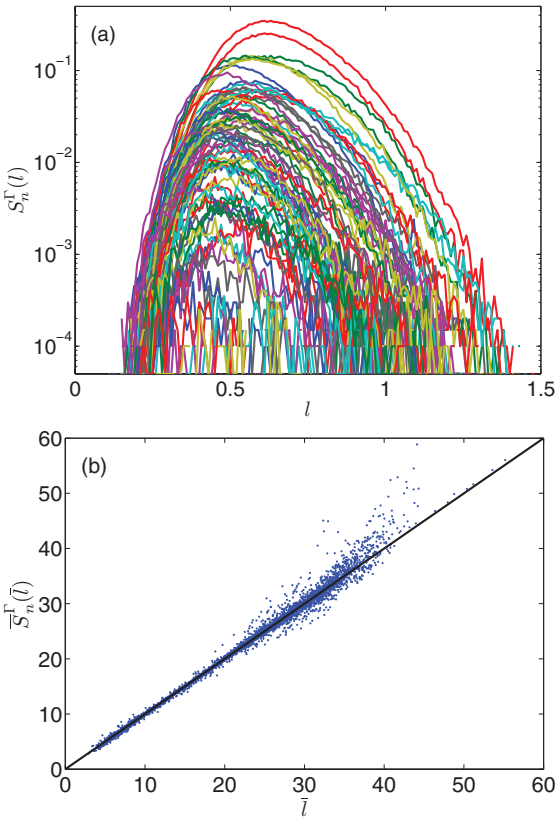

FIG. 8. (Color online) (a) The weighted basin profile functions $S_n^\Gamma(l)$ (for each of the $\mathcal{N}_s = 80$ distinct MS packings for $N = 6$) sampled on hyperspherical shells a distance l from MS packing n using method 2 with $\widetilde{b} = 1$. (b) The scaled weighted basin profile function $\overline{S}_n^\Gamma(\bar{l}) = [S_n^\Gamma(l)\theta\Gamma(k)e^{-l/\theta}]^{1/(k-1)}$ plotted versus the scaled distance $\bar{l} = l/\theta$ obtained from nonlinear least-squares fits to the data in (a) for k and θ. The solid line has slope 1 and zero vertical intercept.

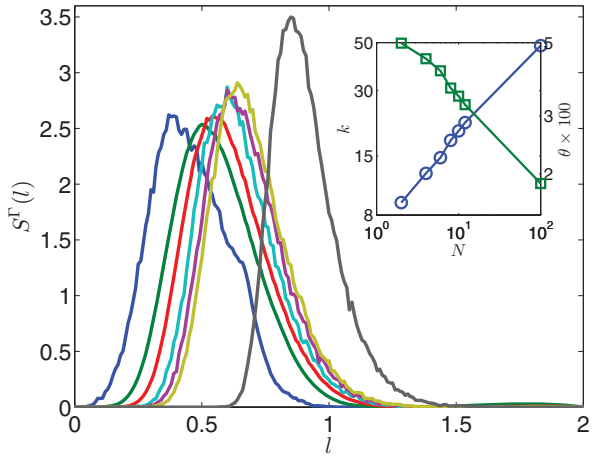

FIG. 9. (Color online) The average weighted basin profile function $S^\Gamma(l)$ for several system sizes $N = 2$, 4, 6, 8, 10, 12, and 100 (from left to right) for damping parameter $\widetilde{b} = 1$. The inset shows the parameters k (circles; left axis) and 100θ (squares; right axis) that describe fits of $S^\Gamma(l)$ to the Γ distribution [Eq. (7)] versus N on a log-log scale.

form of $S_n^\Gamma(l)$ is described by a Γ distribution,

$$S_n^\Gamma(l) = \frac{\left(\frac{l}{\theta}\right)^{k-1} e^{-\frac{l}{\theta}}}{\theta\Gamma(k)}, \tag{7}$$

where $\theta = (\langle l^2\rangle - \langle l\rangle^2)/\langle l\rangle$, $k = \langle l\rangle/\theta$, and $\langle l\rangle = \int_0^\infty dl\, l S_n^\Gamma(l)$. The scaled weighted basin profile functions $\overline{S}_n^\Gamma(\bar{l}) = [S_n^\Gamma(l)\theta\Gamma(k)e^{-l/\theta}]^{1/(k-1)}$ for all microstates collapse when plotted versus the scaled distance $\bar{l} = l/\theta$. The wider scatter at large $\bar{l}$ is caused by undersampling low probability configurations. We find similar quality for the collapse at larger N.

We investigate the system size dependence of the average weighted basin profile function,

$$S^\Gamma(l) = \sum_{n=1}^{\mathcal{N}_s} P_n^\Gamma S_n^\Gamma(l), \tag{8}$$

in Fig. 9 over the range $N = 2{-}100$. $S^\Gamma(l)$ shifts to larger l with increasing N; the peak position k increases by a factor of 5 and scales roughly as $\sqrt{N}$ over this range in N. The width θ slightly narrows over the same range of N, scaling roughly as $N^{-1/4}$.

We also investigated the protocol dependence of the basin profile functions by varying the damping parameter [$\widetilde{b}$ in Eq. (1)] used in the packing-generation procedure for method 2. In the top panel of Fig. 10, we plot the average weighted basin profile function versus the damping parameter over three orders of magnitude in $\widetilde{b}$ from 10^{-2} to 10 for $N = 4$. We were able to saturate the $\widetilde{b}$ dependence of $S^\Gamma(l)$ for both large and small $\widetilde{b}$, that is, for $\widetilde{b} < 10^{-2}$ and $\widetilde{b} > 10$, $S^\Gamma(l)$ is very weakly dependent on $\widetilde{b}$. The two parameters k and θ that describe the shape of $S^\Gamma(l)$ exhibit two key features in the bottom panel of Fig. 10: (1) The peak of the distribution (captured by k) and thus the length scales that determine the MS packing probabilities increase with decreasing $\widetilde{b}$ and (2) the variance (relative to the average) depends weakly on $\widetilde{b}$, but does possess

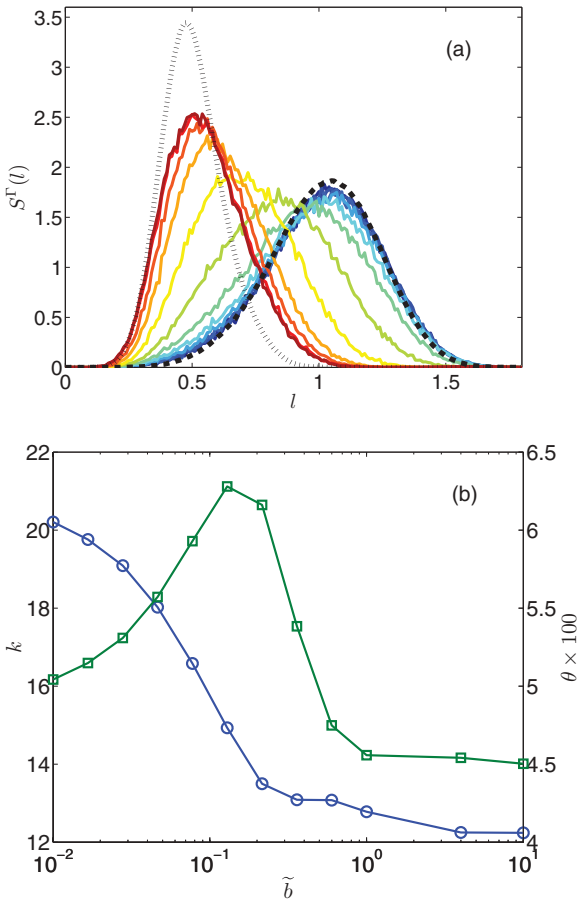

FIG. 10. (Color online) (a) The average weighted basin profile function $S^\Gamma(l)$ for $N = 4$ plotted over a wide range of the damping coefficients $\widetilde{b}$ employed in method 2. $\widetilde{b}$ ranges from 0.01 to 10 from left to right. The thin dotted line gives the probability distribution that a random point in configuration space is a distance l from the nearest permutation and polarization of any MS packing. The thick dotted line is the probability distribution that a random point in configuration space is a distance l from a particular permutation and polarization of the MS packing found in the lower left panel of Fig. 2, which is the most probable MS packing for small $\widetilde{b}$. (b) The parameters k (circles; left axis) and 100θ (squares; right axis) that describe fits of $S^\Gamma(l)$ in (a) to the Γ distribution [Eq. (7)] versus $\widetilde{b}$.

a small peak near $\widetilde{b} = 10^{-1}$. We expect the monotonic increase of k (average l) with decreasing $\widetilde{b}$ to persist for large N.

We are able predict $S^\Gamma(l)$ in the limits of large and small $\widetilde{b}$. Lowering $\widetilde{b}$ decreases the rate at which energy is removed from the system and allows the system to explore larger regions of configuration space. The thick dotted line gives the probability distribution that a random point in configuration space is a distance l from a particular permutation and polarization of the MS packing found in the lower left panel of Fig. 2, which is the most probable MS packing for small $\widetilde{b}$. This distribution matches $S^\Gamma(l)$ for $\widetilde{b} \to 0$. In contrast, larger $\widetilde{b}$ increases the rate at which energy is removed from the system, and thus the initial configurations are typically closer to the final MS packings. The thin dotted line in Fig. 10, which shows the probability distribution that a random point in configuration space is a distance l from the nearest permutation and polarization of any MS packing, gives a similar distribution to $S^\Gamma(l)$ in the

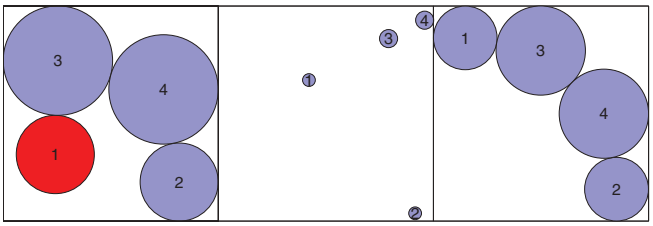

FIG. 11. (Color online) Example of a case when an initial condition for the $N = 4$ system (center) does not map to the closest MS packing (right) via steepest descent ($\widetilde{b} \to \infty$) (left).

large $\widetilde{b}$ limit. The small deviation is due to the fact that some points in configuration space cannot map to the nearest MS packing due to steric constraints (see Fig. 11).

IV. CONCLUSIONS

In this manuscript, we described and carried out a novel computational method for calculating the volume of the MS packing "basins of attraction," which we define as the collection of initial points in configuration space at *zero packing fraction* that map to a given MS packing by following a particular dynamics in the density landscape. Note that our definition of the basin of attraction is protocol dependent, and thus the basin volume will vary with the rate at which energy is dissipated, the compression rate, and other parameters. Using dilute configurations as initial conditions, preventing particle overlaps, and including variations in the basin volume with changes in the packing-generation protocol are crucial for understanding the protocol-dependent structural and mechanical properties of granular media and other athermal particulate systems.

Our computational studies of the basin volumes of MS packings have uncovered three important results: (1) A small approximately hyperspherical region of the basin of attraction with radius l_c surrounds each MS packing, but the volume of this region (relative to $V_{\rm tot}$) is much smaller and only very weakly correlated with the MS packing probabilities in contrast to previous studies of jammed systems [16]; (2) the probabilities of MS packings initialized with dilute configurations are instead controlled by features of the basins of attraction at length scales much further from the MS packing than the core region. In addition, the length scales that control the MS packing probabilities grow with increasing system size and decreasing damping parameter $\widetilde{b}$; and (3) the shape of the basin profile functions are well characterized by Γ distributions, which can be reconstructed by considering distances between random points in configuration space in the limits of large and small $\widetilde{b}$.

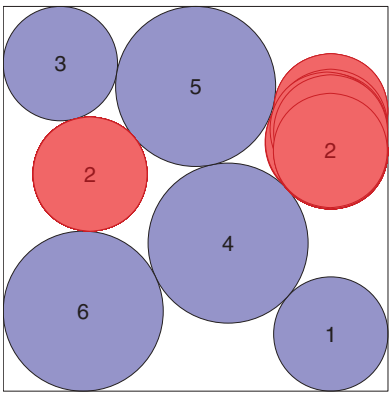

FIG. 12. (Color online) 113 snapshots of one of the $N = 6$ mechanically stable packings (shaded gray in Fig. 3) generated from independent random initial conditions. This packing contains one rattler particle (labeled 2) that can be positioned in the cavity on the left or right and at multiple positions in the right cavity.

Our results suggest a number of promising future studies to better understand the geometrical features of basin volumes. For example, the current studies focused on calculating basin volumes for MS packings initialized at zero packing fraction. We propose to calculate the basin profile functions as a function of the initial packing fraction ϕ_i, and identify the characteristic packing fraction ϕ_i^* above which packing probabilities are determined by the hyperspherical core region of the basin volume. Second, we will perform powerful computational homology (Betti number [26]) and geometry techniques (Laplacian eigenmaps [27]) to characterize the structure of basin volumes as a function of distance l from the MS packing.

We emphasize that there are several key steps in developing a "bottom-up" statistical mechanics description of MS packings: (1) understand the geometrical properties of the MS packing basins of attraction, (2) relate the geometrical

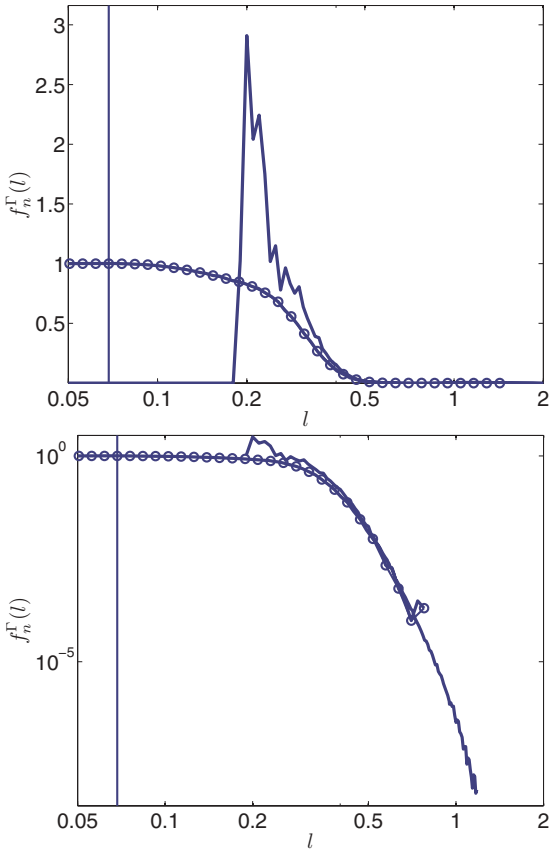

FIG. 13. (Color online) The basin profile function $f_n^\Gamma(l)$ on linear-log (top) and log-log (bottom) scales measured using methods 1 (circles) and 2 (solid lines) for the MS packing in Fig. 12 for $\widetilde{b} = 1$. The vertical lines indicate l_c.

features of the basins of attraction to real-space properties of the MS packings on the particle scale, and (3) coarse-grain this description to predict bulk properties, such as the elastic moduli and yield stress. This manuscript has contributed to the first of these steps.

ACKNOWLEDGMENTS

This research was supported by the National Science Foundation under Grants No. CBET-0967262 (S.A., J.B., C.O.) and No. CBET-0968013 (S.A., M.S.).

APPENDIX: RATTLER PARTICLES

As shown in Figs. 2 and 3, MS packings contain rattler particles. Two of the $\mathcal{N}_s = 6$ distinct MS packings for $N = 4$ and 24 of the $\mathcal{N}_s = 80$ distinct MS packings for $N = 6$ contain rattler particles. For these small-N systems, the fraction of MS packings that contain rattlers is larger than the fraction of particles (roughly 5%–10%) that are rattlers in large MS packings [22]. These previous results suggest that the number of MS packings containing rattlers is extensive with $\mathcal{N}_s$ [28]. How do rattler particles affect the calculation of the basins of attraction for MS packings?

We find that the correspondence between the unweighted $f_n^\Gamma(l)$ and weighted $S_n^\Gamma(l)$ basin profile functions breaks down for small l for MS packings that contain rattler particles. As shown in Fig. 12, for MS packings containing rattlers it is difficult to define uniquely the distance from the initial state to the final MS packing because the rattler particle can exist over a range of positions for a given distinct MS packing. Further, the different rattler locations may give widely varying contributions to the MS packing probability.

In Fig. 13, we plot $f_n^\Gamma(l)$ calculated using methods 1 (circles) and 2 (solid lines) for the MS packing depicted in Fig 12. As described in Sec. III, for method 1, we measure the fraction of times the system returns to the initial MS packing after a perturbation of size l, which is largely unaffected by the presence of rattlers. For method 2, we measure the normalized distribution of distances between the initial configurations and the final MS packings. For large l, method 2 is also largely unaffected by the presence of rattlers. However, when the initial configuration and final MS packing are close together (i.e., small l), the fact that the rattler is not always in the same position in the final MS packing leads to a significant error in measuring l and hence $f_n^\Gamma(l)$, as shown in Fig. 13. For our measurements of basin volumes at small l, such as V_n^c in Fig. 7, we show results using method 1. Our main results are insensitive to the presence of rattler particles because MS packing probabilities (generated from initially dilute configurations) are determined by features of $f_n^\Gamma(l)$ at large l.

[1] G. Y. Onoda and E. G. Liniger, Phys. Rev. Lett. **64**, 2727 (1990).
[2] S. Torquato, T. M. Truskett, and P. G. Debenedetti, Phys. Rev. Lett. **84**, 2064 (2000).
[3] E. R. Nowak, J. B. Knight, E. Ben-Naim, H. M. Jaeger, and S. R. Nagel, Phys. Rev. E **57**, 1971 (1998).
[4] P. Richard, M. Nicodemi, R. Delannay, P. Ribiére, and D. Bideau, Nat. Mater. **4**, 121 (2005).
[5] T. S. Majmudar and R. P. Berhinger, Nature (London) **435**, 1079 (2005).
[6] G. R. Farrell, K. M. Martini, and N. Menon, Soft Matter **6**, 2925 (2010).
[7] K. L. Johnson, *Contact Mechanics* (Cambridge University Press, New York, 1987).
[8] N. Xu, J. Blawzdziewicz, and C. S. O'Hern, Phys. Rev. E **71**, 061306 (2005).
[9] The density landscape is the surface defined by the minimum specific volume (or inverse packing fraction) allowed for each configuration of hard particles.
[10] F. H. Stillinger and T. A. Weber, J. Chem. Phys. **83**, 4767 (1985).
[11] G.-J. Gao, J. Blawzdziewicz, and C. S. O'Hern, Phys. Rev. E **74**, 061304 (2006).
[12] G.-J. Gao, J. Blawzdziewicz, and C. S. O'Hern, Phys. Rev. E **80**, 061303 (2009).
[13] C. E. Zachary, Y. Jiao, and S. Torquato, Phys. Rev. E **83**, 051308 (2011).
[14] M. Clusel, E. I. Corwin, A. O. N. Siemens, and J. Brujic, (London) Nature **460**, 611 (2009).
[15] F. H. Stillinger and T. A. Weber, Science **225**, 983 (1984).
[16] N. Xu, D. Frenkel, and A. J. Liu, Phys. Rev. Lett. **106**, 245502 (2011).
[17] N. Ch. Karayiannis and M. Laso, Phys. Rev. Lett. **100**, 050602 (2008).
[18] R. S. Hoy and C. S. O'Hern, Phys. Rev. Lett. **105**, 068001 (2010).
[19] L. M. Lopatina, C. J. Olson Reichhardt, and C. Reichhardt, Phys. Rev. E **84**, 011303 (2011).
[20] L.-N. Zou, X. Cheng, M. L. Rivers, H. M. Jaeger, and S. R. Nagel, Science **326**, 408 (2009).
[21] L. Berthier, H. Jacquin, and F. Zamponi, Phys. Rev. E **84**, 051103 (2011).
[22] C. S. O'Hern, L. E. Silbert, A. J. Liu, and S. R. Nagel, Phys. Rev. E **68**, 011306 (2003).
[23] T. Aste and T. Di Matteo, Phys. Rev. E **77**, 021309 (2008).
[24] F. Lechenault, F. da Cruz, O. Dauchot, and E. Bertin, J. Stat. Mech. (2006) P07009.
[25] A. Panaitescu and A. Kudrolli, Phys. Rev. E **81**, 060301(R) (2010).
[26] L. Kondic, A. Goullet, C. S. O'Hern, M. Kramar, K. Mischaikow, and R. P. Behringer, Europhys. Lett. **97**, 54001 (2012).
[27] M. Belkin and P. Niyogi, Neural Comput. **15**, 1373 (2003).
[28] A. Donev, S. Torquato, and F. H. Stillinger, Phys. Rev. E **71**, 011105 (2005).